*Carcinogenesis*, 2021, Vol. 42, No. 3, 357–368

**doi:10.1093/carcin/bgaa139**
Advance Access publication December 21, 2020
Original Article



ORIGINAL ARTICLE

# NFIA and NFIB function as tumour suppressors in high-grade glioma in mice

Kok-Siong Chen[1,†], Zorana Lynton[1,2,†], Jonathan W.C.Lim[1], Thomas Robertson[2,3], Richard M.Gronostajski[4], Jens Bunt[1,6,‡,*] and Linda J.Richards[1,5,‡,*]

[1]The Queensland Brain Institute, The University of Queensland, Brisbane, Queensland 4072, Australia, [2]Faculty of Medicine, The University of Queensland, Brisbane, Queensland 4072, Australia, [3]Anatomical Pathology, Pathology Queensland, Royal Brisbane and Women's Hospital, Brisbane, Queensland 4029, Australia, [4]Department of Biochemistry, Program in Genetics, Genomics and Bioinformatics, Center of Excellence in Bioinformatics and Life Sciences, State University of New York at Buffalo, Buffalo, NY 14203, USA and [5]School of Biomedical Sciences, The University of Queensland, Brisbane, Queensland 4072, Australia

[6]Current address: Princess Maxima Center for Pediatric Oncology, Utrecht 3584 CS, the Netherlands.
[†]These authors contributed equally to this work.
[‡]Equal senior authors.
*To whom correspondence should be addressed. Tel: +61 7 3346 6335; Email: j.bunt-7@prinsesmaximacentrum.nl
Correspondence may also be addressed to Linda J. Richards. Tel: +61 7 3346 6335; Email: richards@uq.edu.au

## Abstract

Nuclear factor one (NFI) transcription factors are implicated in both brain development and cancer in mice and humans and play an essential role in glial differentiation. *NFI* expression is reduced in human astrocytoma samples, particularly those of higher grade, whereas over-expression of NFI protein can induce the differentiation of glioblastoma cells within human tumour xenografts and in glioblastoma cell lines *in vitro*. These data indicate that NFI proteins may act as tumour suppressors in glioma. To test this hypothesis, we generated complex mouse genetic crosses involving six alleles to target gene deletion of known tumour suppressor genes that induce endogenous high-grade glioma in mice, and overlaid this with loss of function *Nfi* mutant alleles, *Nfia* and *Nfib*, a reporter transgene and an inducible Cre allele. Deletion of *Nfi* resulted in reduced survival time of the mice, increased tumour load and a more aggressive tumour phenotype than observed in glioma mice with normal expression of NFI. Together, these data indicate that *NFI* genes represent a credible target for both diagnostic analyses and therapeutic strategies to combat high-grade glioma.

## Introduction

High-grade gliomas comprise the most common primary malignant brain tumours and have lagged behind other cancers with regards to the development of therapeutic interventions (1). To discover more effective treatments a better understanding of their pathophysiology is essential. As these tumours resemble cells of glial lineage, they share many processes and regulatory pathways with normal gliogenesis (2).

The nuclear factor one (NFI) transcription factors are important regulators of normal glial differentiation and impact glioma outcomes. Developmentally, knockout mouse models for these genes display delayed and reduced differentiation of both neurons and glia which in turn affects overall brain development and function (3–7). The essential function of family members NFIA and NFIB in astrocytic differentiation was underscored when they were identified as critical drivers of differentiation in induced pluripotent stem cells *in vitro* (8,9). In glioma, an increasing body of work has demonstrated that both NFIA and NFIB retain their function as essential drivers of glial differentiation, and thus may impact the pathophysiology of the disease through similar mechanisms (10–15).

**Received:** July 30, 2020; **Revised:** December 5, 2020; **Accepted:** December 18, 2020

**Abbreviations**

| | |
|---|---|
| HGA | high-grade astrocytoma |
| LOH | loss of heterozygosity |
| NFI | nuclear factor one |
| PBS | phosphate-buffered saline |
| PFA | paraformaldehyde |
| ROI | region of interest |

NFIs have been increasingly studied in glioma and may have an endogenous tumour suppressive function. Indeed, *NFI* mRNA expression is negatively correlated with tumour grade, as is NFIA at the protein level (10,14,16). Conversely, high *NFI* expression is associated with improved survival from brain cancer (10,14,16). On a cellular level, NFIA and NFIB expression in glioblastoma cells is correlated with co-expression of glial differentiation genes, but not proliferative genes (14). While these results provide evidence for tumour suppressive potential of NFIs, there is also research that suggests an oncogenic potential in glioma (10,17–19). NFIs may therefore be dependent on context-specific factors as they demonstrate paradoxical roles in many cancers (20). Thus, systematic manipulation in a context-controlled model is necessary to examine the role of NFIs in glioma pathophysiology.

NFIs have also been implicated in comprehensive studies of molecular pathogenesis. In a handful of studies, haploinsufficiency of *NFIB* as part of loss of heterozygosity (LOH) of chromosome 9p was very common (21). Copy number predictions in the Cancer Genome Atlas data suggest that a copy of *NFIB* is deleted in approximately 30% of grade II astrocytoma to 50% of grade IV glioblastoma (22–24). Additionally, loss of *NFIA* is predicted in 3–5% of some gliomas, commonly as part of a larger deletion of chromosome 1p (22–24). As these large deletions affect many other genes, it remains unclear whether deletion of *NFIA* or *NFIB* has an impact on tumour progression or aggressiveness.

Insertional mutagenesis mouse models suggest an independent role for *Nfi* in tumorigenesis. Across multiple studies, insertions in the *Nfi* genes were amongst the most common and observed in 8 out of 108 (7%) and 4 out of 33 (12%) gliomas (25,26). Interestingly, 2 out of 6 glioblastomas contained an insertion in *Nfia* or *Nfib*, further indicating that disrupting NFI levels may favour increased grading and aggressiveness (26). However, as each tumour harbours multiple insertions, these studies are limited in their ability to determine the individual effect of *Nfi* disruption and its contribution to tumour progression or behaviour.

To determine whether NFIA and NFIB proteins have an intrinsic tumour suppressive role in context-controlled experiments, we generated high-grade astrocytoma (HGA) models with conditional deletion of *Nfia* or *Nfib*. Knockout of either *Nfi* resulted in reduced latency and in increased tumour load as more and larger tumours were observed. These observed tumours closely modelled human glioblastoma pathology. They were less differentiated, contained more irregular, hyperchromatic nuclei and had more diffuse borders, suggesting a more aggressive pathology resulting from *Nfi* deletion.

## Materials and methods

### Animals

To generate HGA mouse models, the previously described HGA mouse model *Pten*$^{tm2MAK}$; *Rb1*$^{tm2Brn}$; *Trp53*$^{tm1Brn}$; Tg(GFAP-cre/Esr1*,-lacZ)$^{BSbk}$ was crossed with the Cre recombinase-mediated tdTomato reporter line *Gt(ROSA)26Sor*$^{tm14(CAG-tdTomato)Hze}$ (27–30). The resulting model was designated as HGA-Control. To generate HGA mouse models with conditional deletion of *Nfia* (HGA-Nfia$^{flox}$) or *Nfib* (HGA-Nfib$^{flox}$), the *Nfia*$^{tm2Rmg}$ or *Nfib*$^{tm2.1Rmg}$ allele was crossed in, respectively (31–33). These mice were maintained on a predominantly FVB/NJ background with contributions from 129/SV and C57Bl6. All breeding and experiments were performed at The University of Queensland in accordance with the Australian Code of Practice for the Care and Use of Animals for Scientific Purposes, and with the approval from The University of Queensland Animal Ethics Committee. All animals were housed on a 12-h dark/light cycle with water and food provided *ad libitum*.

### Generation and collection of tumours in mice

To induce tumour formation in HGA-Control, HGA-Nfia$^{flox}$ and HGA-Nfib$^{flox}$ mice, Cre recombinase was activated by intraperitoneal injection of up to 150 µl of 20 mg/ml tamoxifen (Sigma-Aldrich, St Louis, MO) dissolved in corn oil (Sigma-Aldrich) in four- to six-week-old mice once a week for three consecutive weeks. Only male animals were used in analyses, as females displayed tamoxifen-induced mammary glands problems. Animal health and welfare was monitored up to twice daily, with clinical signs monitored with a scoresheet. Clinical signs included changes in general appearance, digestion, behaviour or specific clinical signs of glioblastoma. Animals were euthanised based on morbidity requirement, which this study defines as the clinical endpoint, or 17–80 days after the first tamoxifen injection for assessment of tumour initiation. Survival was calculated from the first day of tamoxifen injection to the clinical endpoint and from the first day of clinical signs to the clinical endpoint. Where animals were euthanised on the same day as clinical signs first appeared, the animal was considered to have one day of clinical signs. Mice euthanised for non-tumour related reasons were excluded from analyses. Mice were transcardially perfused with saline, followed by 4% w/v paraformaldehyde (PFA) in phosphate buffered saline (PBS; Lonza, Basel, Switzerland). The brains were then dissected and post-fixed in 4% PFA at 4°C for up to one week.

### Tissue processing

Following post-fixation, mouse brain tissue was embedded in 3–4% w/v Difco Noble agar (Becton, Dickinson and Company, Sparks, MD) in distilled water, and sectioned at 50 µm coronally on a vibratome (Leica, Wetzlar, Germany). Sections were stored in PBS with 0.2% w/v sodium azide at 4°C or mounted directly onto Superfrost Plus slides (Menzel-Gläser, Brunswick, Germany), and dried at room temperature until fully adhered. Sections were post-fixed with 4% PFA for 10 min and washed with PBS for five minutes. For immunofluorescence, antigen retrieval was performed in an antigen decloaking chamber (Biocare Medical, Concord, CA). The sections were heated to 125°C for four minutes at 15 psi in sodium citrate buffer (10 mM $C_6H_5Na_3O_7$, 0.05% v/v Tween 20 in MilliQ $H_2O$, pH 6.0), and then washed with PBS prior to immunohistochemistry.

### Histology and immunohistochemistry

To determine tumour load and pathology, every sixth coronal section of each brain was mounted and stained with Ki76 using a chromogenic immunohistochemistry method and counterstained with haematoxylin and eosin (H&E). The method was conducted as follows: upon antigen retrieval, sections were incubated for two hours in blocking solution containing 2% v/v normal donkey serum (Jackson Laboratories, West Grove, PA), 0.9% hydrogen peroxide ($H_2O_2$; Chem-Supply, Adelaide, Australia) and 0.2% v/v Triton X-100 (Sigma-Aldrich) in PBS. Subsequently, sections were incubated overnight with a mouse anti-Ki67 antibody (1:200, BD Biosciences, Sparks, MD, Cat# 550609) diluted in 2% v/v normal donkey serum and 0.2% Triton X-100 in PBS. Sections were washed in PBS for 3 × 20 min before incubating for one hour with biotinylated donkey anti-mouse IgG (1:500, Jackson Laboratories) diluted in 0.2% v/v Triton X-100 in PBS. Sections were washed as previous, and then incubated for one hour in an avidin-biotin complex solution (0.2% v/v Triton X-100, avidin [1:500] and biotin [1:500] from a Vectastain™ Elite ABC kit [Vector Laboratories] diluted in PBS). After additional washes, sections were incubated with Ni-DABchromogen solution (95 mM $NiSO_4$, 175 mM sodium acetate, 0.56 mM 3,3′-diaminobenzidine tetrahydrochloride [Sigma-Aldrich],

0.00075% $H_2O_2$). Sections were observed until staining was visible, after which the reaction was stopped via PBS wash. After additional washes, sections were dehydrated by transferring through a series of ethanol (70–100%) and xylene washes, for at least two minutes each. Slides were coverslipped with DPX neutral mounting medium (Ajax Finechem, Sydney, Australia).

Fluorescence immunohistochemistry was conducted as follows: upon antigen retrieval, sections were incubated for two hours in blocking solution containing 10% v/v normal donkey or goat serum (Jackson Laboratories, West Grove, PA), 0.9% hydrogen peroxide] and 0.2% v/v Triton X-100 in PBS. Subsequently, sections were incubated overnight with primary antibody diluted in 2% v/v normal serum and 0.2% Triton X-100 in PBS. Primary antibodies and the concentrations used were: rabbit anti-NFIA (1:500, Sigma-Aldrich, Cat# HPA008884), rabbit anti-NFIB (1:500, Sigma-Aldrich, Cat# HPA003956), biotinylated rabbit anti-NFIA (1:500, LifeSpan BioSciences, Cat# LS-C428417), rabbit anti-NFIB Alexafluor 448 (1:500, Abcam, Cat# ab216931), chicken anti-GFAP (1:1000, Abcam, Cat# ab4674), goat anti-tdTomato (1:1000, SICGEN, Cat# AB8181-200), mouse anti-S100B (1:500, Abcam, Cat# ab4066) and rabbit anti-phosphoHistone H3 (Ser10; 1:500, Cell Signaling, Cat#53348).

Sections were washed in PBS for 3 × 20 min before incubating with secondary antibody. The secondary antibodies used were either donkey anti-rabbit IgG, donkey anti-mouse IgG, donkey anti-goat IgG or donkey anti-chicken IgG conjugated with Alexafluor 488 or 555 (1:500; Invitrogen, Melbourne, Australia) diluted in PBS containing 0.2% v/v Triton X-100, and incubated for three hours in a light protected humidified chamber. For fluorescence streptavidin amplification, the sections were incubated with 1:500 diluted biotinylated donkey anti-rabbit IgG, anti-chicken IgG or anti-mouse IgG secondary antibody (Jackson Laboratories) for 1 h. After 3 × 10 min washes with PBS, the sections were incubated with Strepavidin-647 conjugate amplification reagent (1:500; Invitrogen) diluted in 0.2% Triton X-100 in PBS for 1 h.

### Image acquisition and analyses

Large-scale brightfield imaging for slides with H&E staining was performed with a Zeiss upright Axio-Imager Z2 microscope fitted with Metasystems-Coolcube1 cameras, and captured with Metafer VSlide software (Metasystems, Boston, US). Tumour masses in H&E-stained sections were identified through manual observation. To estimate tumour size, the maximal surface area from H&E-stained coronal sections was measured for each tumour mass using FIJI (34). Nuclear atypia, a characteristic correlated with the 2016 WHO histological grading of diffuse astrocytic tumours, was inferred by quantification of hyperchromatic nuclei. Cells with hyperchromatic nuclei were quantified for each tumour within a region of interest (ROI) measuring 1500 × 1500 μm using Imaris. Hyperchromatic nuclei were defined as spots with a diameter larger than 30 μm that were stained with haematoxylin. Each section was then inspected manually to discount potential false positives. The number of tumours demonstrating invasion into normal brain tissue was determined by visually inspecting each series of H&E-stained coronal sections.

High resolution fluorescence images were collected using a Diskovery spinning disk confocal system (Spectral Applied Research Inc, Ontario, Canada) built around a Nikon TiE body and equipped with two sCMOS cameras (Andor Zyla 4.2, 2048 × 2048 pixels) and captured with Nikon NIS software (Nikon, Tokyo, Japan). Images were pseudocoloured to permit overlay, cropped, sized, and contrast-brightness enhanced for presentation with Adobe Photoshop and Illustrator software. Semi-automated cell counting of fluorescent images was performed using Imaris software (Bitplane, Zürich, Switzerland), version 8.2.1 and above. Counts for pH3- or S100B-positive cells were first performed using an automatic built-in spot detection algorithm in the Imaris software within three non-necrotic 500 × 500 μm ROIs. Positive signals within the ROI with a diameter larger than 10 μm that co-localised with DAPI were defined as positive counts. This algorithm was similarly used to determine the co-localisation of double-labelled cells. Two spots were considered co-localised if the distance between their centre was less than or equal to 6 μm. Overlapping signals were subsequently validated by visual inspection to discount potential false positives. Colocalisation of GFAP, S100B and tdTomato were conducted 1000 μm wide matched cortical regions as previously described (14,35).

### Neuropathology

Tumours were grossly assessed for resemblance to human tumours. H&E stained sections of whole brain series were independently evaluated by a neuropathologist (TR), who was blinded to the mouse model of origin. Tumours were diagnosed according to 2016 World Health Organisation criteria for human high-grade glioma. In particular, the presence of mitoses, necrosis and or vascular proliferation. In addition, a variety of histologic features of aggressiveness were scored as absent (0) or present (1), with some features also including an additional score for abundant (2). These included necrosis (0–2), haemorrhage (0–2), parenchymal invasion (0–2), corpus callosum invasion (0–1), ependymal spread (0–1) and cellular pleomorphism (0–2). Other distinct features were noted.

### *In silico* analyses

Gene correlation analyses were performed using published gene expression data consisting of 14 tumour samples of the original HGA model (GSE22927) (27). This dataset was analysed and visualised using the R2: microarray analysis and visualisation platform (http://r2.amc.nl) as previously described (36). Gene set enrichment analyses were performed using the DAVID online tool and compared to those obtained from human glioblastoma expression datasets TCGA (23), GSE108474 (37) and GSE16011 (38) as previously described (14,39).

### Statistical analysis

Statistical significance for survival of mice from the three HGA models were determined using log-rank tests. Statistical significance for analyses of tumour number, tumour surface area and cell counts were determined using Mann–Whitney *U* tests. For analyses of infiltrative cells at the tumour border, statistical significance was determined using Chi-square tests with Yates' correction. Statistical significance of categorical data obtained from neuropathological examination were determined using Spearman correlation. For analyses of cellular staining in HGA models at different time points, at the tumour border, statistical significance was determined using a two-way ANOVA and Tukey's multiple comparison test.

## Results

### NFIA and NFIB expression in HGA mouse model tumours mimics human tumours

To investigate whether NFI functions as an intrinsic tumour suppressor and how a reduction of endogenous NFI levels affect tumour progression and behaviour, required a model with endogenous tumour development, rather than the commonly used xenograft models. We investigated whether a previously established mouse model for inducible, endogenous HGA would be suitable to study how NFI affects tumour growth (27,40). In this model, deletion of tumour suppressor genes *Pten*, *Rb1* and *Tp53* can be induced in GFAP-positive cells to generate HGA tumours.

We first assessed whether *Nfia* and *Nfib* are co-expressed in tumours generated in these mice by analysing an available mRNA expression dataset for this model (27). Indeed, *Nfia* expression strongly correlated with *Nfib* expression in HGA tumours (Figure 1A), similar to our previous findings in human glioblastoma (14). This also holds true on a protein level as assessed by immunofluorescent co-staining of NFIA and NFIB in tumours, with most tumour cells expressing NFIA also expressing NFIB (Figure 1B).

To determine whether the molecular pathways associated with *Nfia* and *Nfib* expression were similar to those in human tumours, gene ontology analyses were performed for the top 500 genes with positive and negative correlation with *Nfia* and *Nfib* expression, respectively (Table S1, available at *Carcinogenesis* Online). Of the 84 and 105 terms for biological function uniquely enriched in *Nfia* and *Nfib* positively correlated genes with $P < 0.005$, 45 terms were shared between both (Table S2, available at *Carcinogenesis* Online), which is similar to that observed

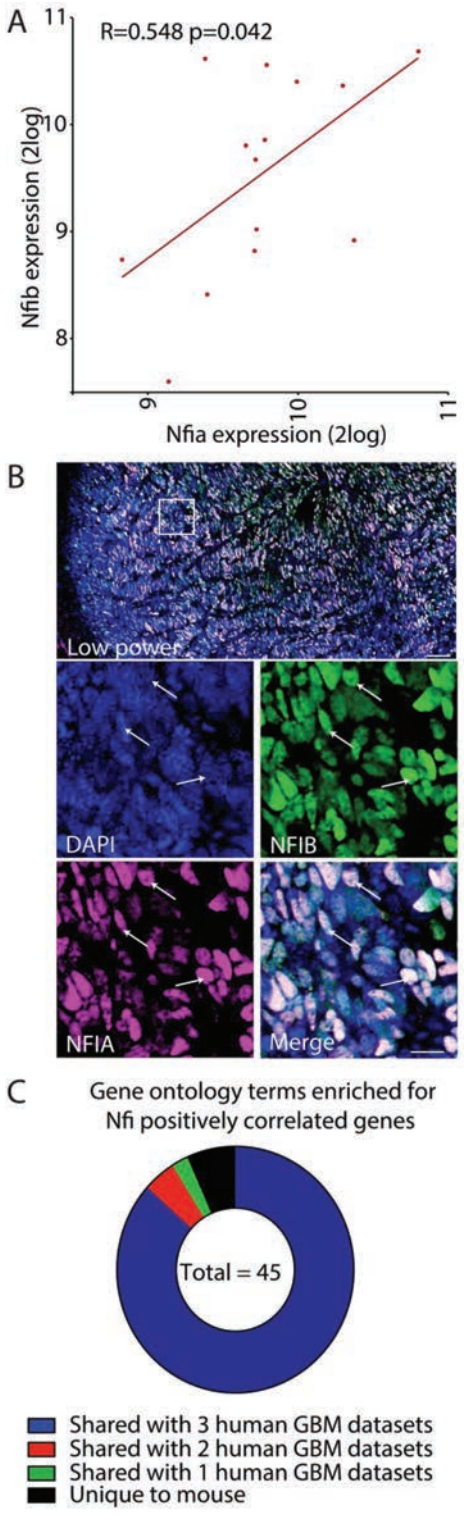


**Figure 1.** NFIA and NFIB expression in tumours arising in high-grade glioma (HGA) models mimic their expression in human glioblastoma. (**A**) Similar to human tumours, mRNA expression of *Nfia* and *Nfib* are strongly correlated in tumours collected from the HGA mouse model (27). (**B**) NFIA and NFIB proteins show cellular colocalisation by immunofluorescent staining of tumours in coronal sections of HGA-control brains ($n$ = 6). (**C**) 45 terms were co-enriched in gene ontology enrichment analyses of the top 500 genes respectively correlated with *Nfia* and *Nfib* expression in HGA-Control tumours. The majority of these are similarly enriched from identical analyses of human glioblastoma (GBM) expression datasets. GBM, glioblastoma. Scale bar in (B) lower power = 200 μm; high power = 50 μm.

in human tumours (14). Furthermore, 41 out of 45 gene ontology terms were shared with at least two of the human glioblastoma expression datasets analysed (Figure 1C). Together, these data indicate that this HGA model mimics NFI expression and function observed in human tumours.

## Generation of mouse models to investigate the role of NFI in high-grade astrocytoma

To delete either *Nfia* or *Nfib* in tumours, we crossed the HGA model with a Cre recombinase-dependent tdTomato reporter line and *Nfia* or *Nfib* conditional alleles (Figure 2A) (27,30,32,33). The resulting models were designated HGA-Nfia$^{flox}$ and HGA-Nfib$^{flox}$, respectively, with HGA-Control representing the control line with wildtype *Nfia* and *Nfib* alleles. Following induction of Cre recombinase activity by tamoxifen administration, expression of the tdTomato reporter protein co-localises with GFAP-positive cells in all three models (Figure 2A–E). As expected based on the normal expression of NFIA and NFIB in the adult cerebral cortex, the tdTomato-positive cells in HGA-Control brains expressed both NFI proteins (35). In the HGA-Nfia$^{flox}$ and HGA-Nfib$^{flox}$ models, NFIA and NFIB staining were, respectively, absent. Consequently, the tumours arising in the latter models were also negative for the deleted *Nfi* family member apart from infiltrating cell types (Figure 2F–H). Tumours in the HGA-control mice expressed both NFIA and NFIB, while the non-affected *Nfi* member was expressed in the other two models.

## Deletion of Nfi results in more and larger tumours

After administration of tamoxifen, the animals from all three HGA models developed tumours (Figure 3A). Similar to the previous study of the HGA model, HGA-Control mice had a median to morbidity of 153 days and developed severe clinical signs warranting euthanasia (27). The median to morbidity for HGA-Nfia$^{flox}$ and HGA-Nfib$^{flox}$ mice was reduced to 140 and 147 days, respectively ($P$ = 0.0009 and 0.1207; Log-rank test; Figure 3B and Table S3A and B, available at *Carcinogenesis* Online). The HGA-Nfia$^{flox}$ model showed quicker disease progression from first presentation of clinical signs compared to HGA-Control ($P$ = 0.0178; Log-rank test), with the median survival from first clinical signs reduced from 13 to 8.5 days in HGA-Control and in HGA-Nfia$^{flox}$, respectively (Figure 3C and Table S3A and C, available at *Carcinogenesis* Online). Disease progression from first presentation of clinical signs was not significantly different in HGA-Nfib$^{flox}$ compared to HGA-Control ($P$ = 0.4361; Log-rank test).

More strikingly, when assessing the number of tumour masses in a series of rostral to caudal coronal sections stained for H&E, both HGA-Nfia$^{flox}$ and HGA-Nfib$^{flox}$ mice displayed a higher number of tumour masses per animal without discernible microscopic connection (Figure 3A and D and Table S4, available at *Carcinogenesis* Online). Whilst most HGA-control brains presented with a single tumour mass, *Nfi* deletion generally resulted in two or more independent masses per animal ($P$ = 0.0282 for HGA-Nfia$^{flox}$ and $P$ = 0.0039 for HGA-Nfib$^{flox}$; Mann–Whitney $U$ test; Figure 3D). As a proxy for tumour size, we quantified the surface area for each individual mass based on the section representing the largest surface area for that mass. For each mouse, the total tumour surface area was doubled in HGA-Nfia$^{flox}$ and HGA-Nfib$^{flox}$ mice compared to HGA-control mice ($P$ = 0.0152 for HGA-Nfia$^{flox}$ and $P$ = 0.0057 for HGA-Nfib$^{flox}$; Mann–Whitney $U$ test; Figure 3E). This observed increase was not solely driven by there being more tumour masses in HGA-Nfia$^{flox}$ and HGA-Nfib$^{flox}$ mice, as the mean size of the largest individual tumour per mouse increased from 18.9 mm$^2$ in HGA-control to 27.1 mm$^2$ in HGA-Nfia$^{flox}$ and to 24.6 mm$^2$ in HGA-Nfib$^{flox}$ mice (Table S4,

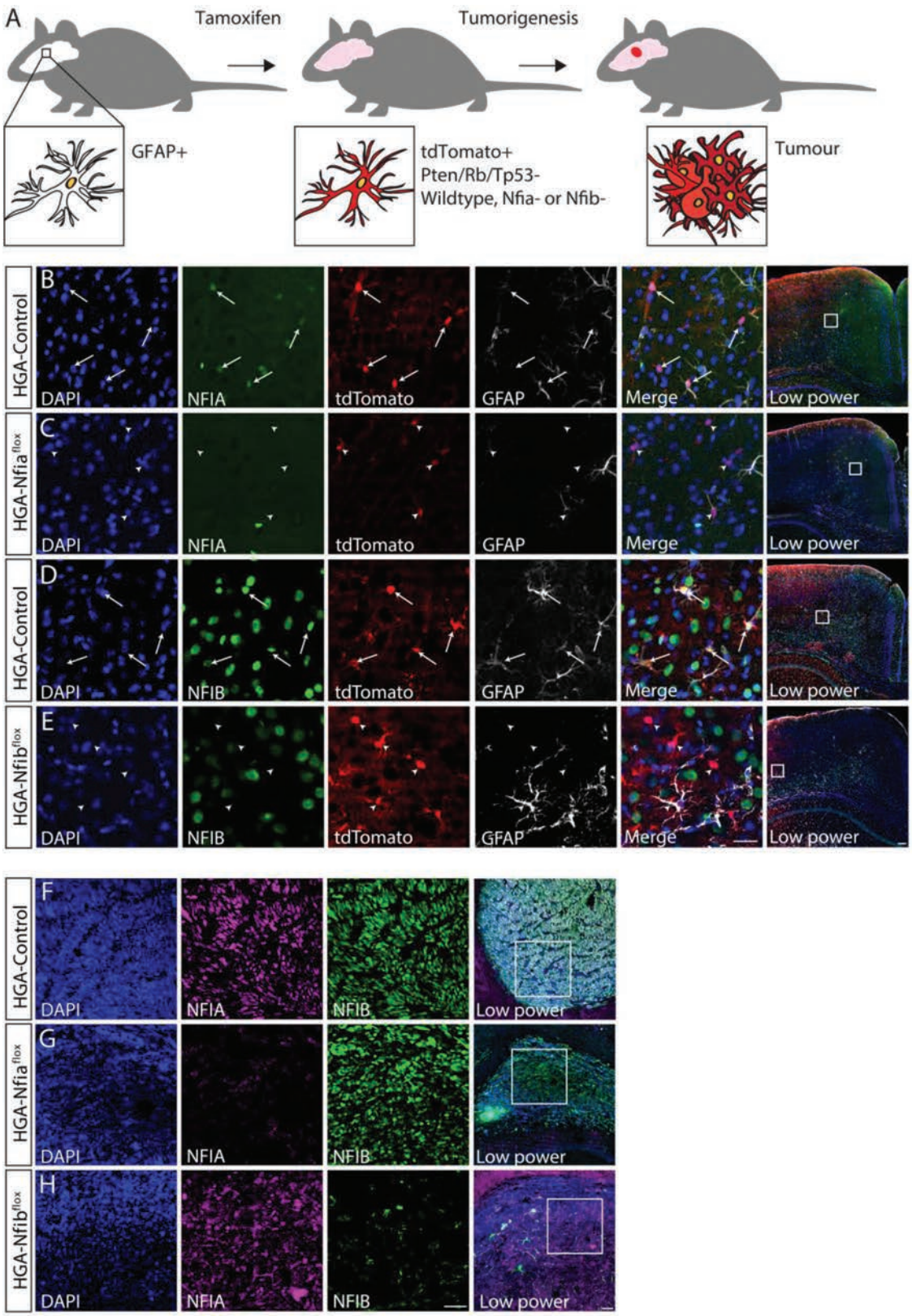


**Figure 2.** High-grade astrocytoma (HGA) models to investigate the role of NFI in tumour progression and behaviour. (**A**) Schematic representation of HGA models. Inducible Cre recombinase is expressed in GFAP-positive cells in the brain. After administration of tamoxifen, Cre recombinase activity results in expression of the red fluorescence marker tdTomato and deletion of the tumour suppressor genes *Pten*, *Rb1* and *Tp53*. *Nfia* and *Nfib* are also deleted in HGA-Nfia$^{flox}$ and HGA-Nfib$^{flox}$, respectively. After induction, high-grade glioma develops. (**B**), (**C**), (**D**) and (**E**) Immunohistochemical analyses of recombination 17 days post injection with tamoxifen in coronal sections of adult mouse brains. In all three HGA models, co-staining of tdTomato and GFAP is observed ($n$ = 6 per model). Furthermore, in HGA-Control NFIA and NFIB expression is detected in tdTomato-positive cells (Arrows in B and D), while no expression of NFIA or NFIB is observed in HGA-Nfia$^{flox}$ and HGA-Nfib$^{flox}$ co-staining, respectively (Arrowheads in C and E). (**F**) Immunohistochemical analyses of endpoint tumours demonstrate both NFIA and NFIB are expressed in HGA-Control brains. (**G**) and (**H**) In contrast, only the non-deleted family member was expressed in HGA-Nfia$^{flox}$ and HGA-Nfib$^{flox}$ tumours ($n$ = 6 per model). Scale bar in (E) high power = 50 μm; low power = 200 μm, in (H) high power = 200 μm; low power = 250 μm

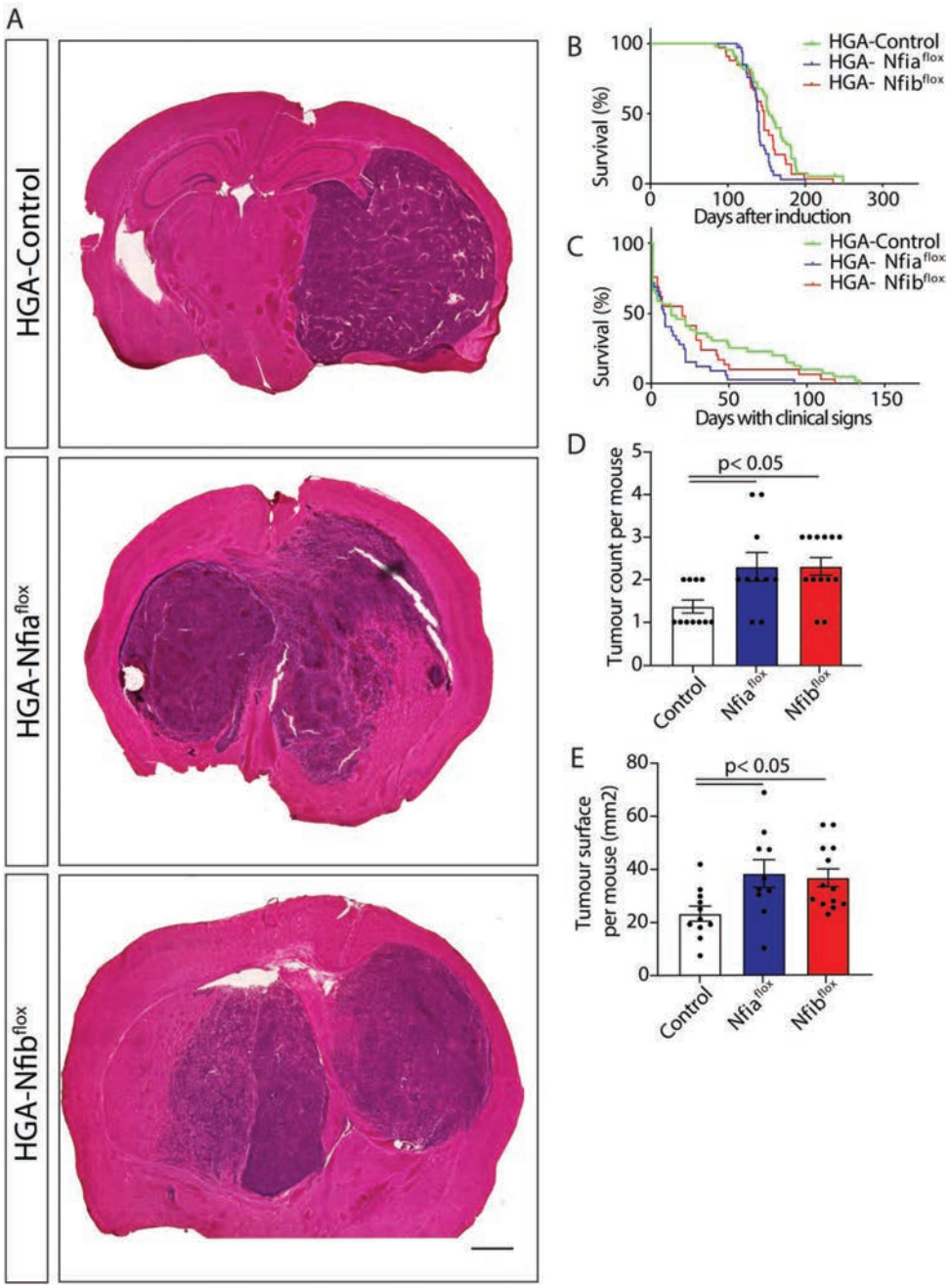


**Figure 3.** Deletion of *Nfia* or *Nfib* leads to increased tumorigenesis. **(A)** Representative sections of tumour masses in HGA-Control, HGA-Nfia$^{flox}$ and HGA-Nfib$^{flox}$. H&E staining was performed on series of coronal sections from brains of the three HGA models. Compared to HGA-Control, which mostly presents with a single well-circumscribed tumour mass, HGA-Nfia$^{flox}$ and HGA-Nfib$^{flox}$ mice display multiple and more diffuse tumour masses. (**B**) Kaplan–Meier curve representing the survival of three HGA models in days after the first administration of tamoxifen up to the time of euthanasia for morbidity. Compared to HGA-Control mice, survival time is decreased in HGA-Nfia$^{flox}$ mice. (**C**) Kaplan–Meier curve representing the survival of HGA mice in days after detection of the first clinical signs. Compared to HGA-control mice, survival is decreased in HGA-Nfia$^{flox}$ mice. (**D**) Using the histological series described in (A), the number of independent tumours was determined for each mouse. Each tumour mass was considered an independent tumour if it was separated from another tumour mass by normal tissue. On average, HGA-Nfia$^{flox}$ and HGA-Nfib$^{flox}$ mice harboured twice as many tumours as compared to HGA-Control. (**E**) As an estimate of total tumour load per mouse, the largest surface of each independent tumour was measured. Compared to HGA-Control mice, mice with deletion of *Nfia* or *Nfib* had a larger total tumour surface area. Scale bar in (A) = 1000 μm. Error bars in (D) and (E) depict mean ± SEM.

available at *Carcinogenesis* Online). Together, these data indicate that loss of *Nfi* increases tumour burden.

## HGA-Nfia$^{flox}$ and HGA-Nfib$^{flox}$ tumours show hallmarks of more aggressive tumours

As NFI expression is important for normal astrocytic differentiation and is associated with differentiated cells in human glioblastoma, we performed immunofluorescent staining for the proliferation marker phosphorylated histone H3 (pH3) and the glial differentiation marker S100B on three independent regions of non-necrotic tissue in the largest tumour observed in each mouse (Figure 4A–C and Table S5, available at *Carcinogenesis* Online) (14). Although both the median and mean number of mitotic pH3 positive cells slightly increased in both HGA-Nfia$^{flox}$

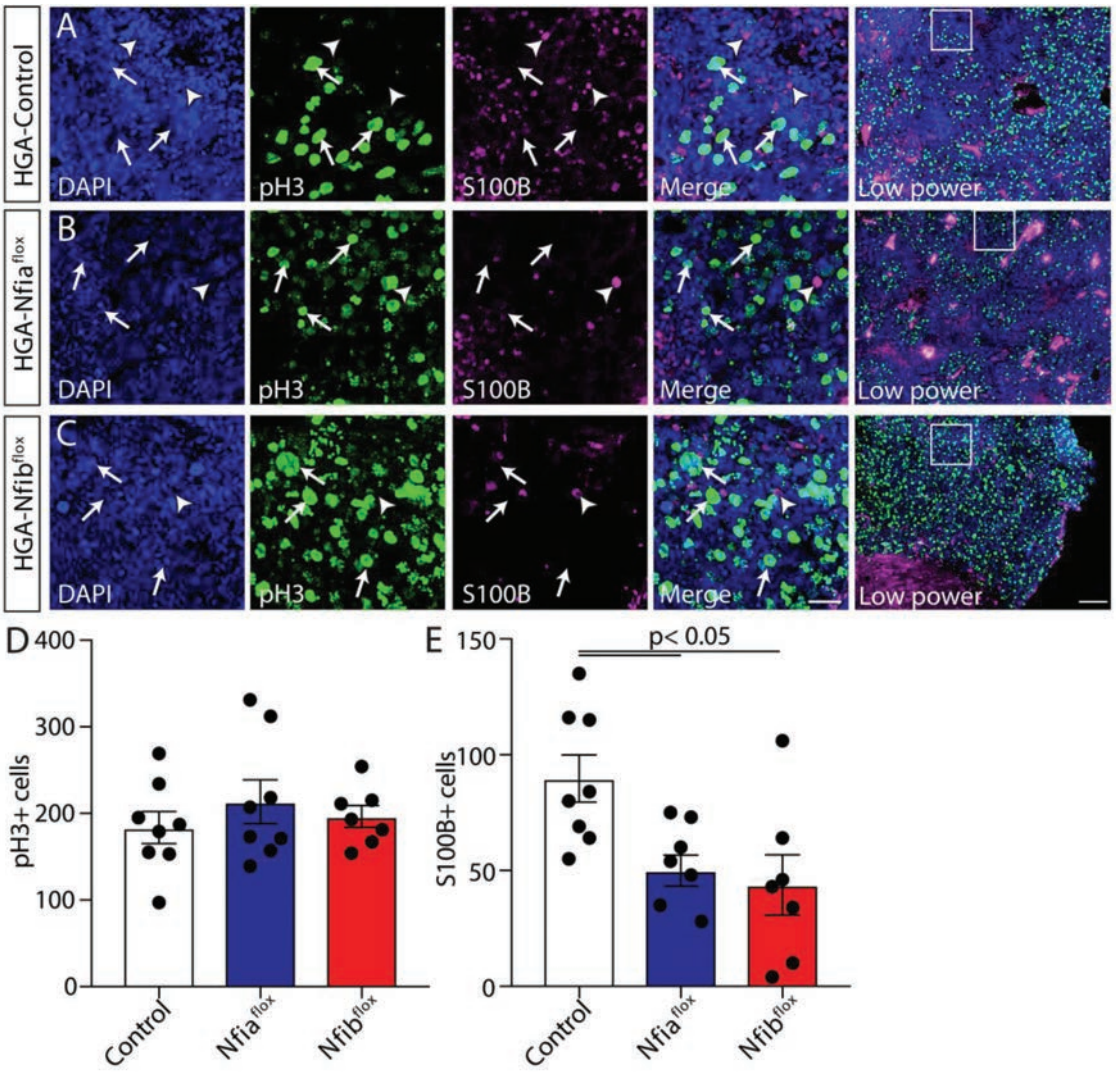


**Figure 4.** HGA-Nfia$^{flox}$ and HGA-Nfib$^{flox}$ tumours have fewer differentiated astrocytes. (**A**), (**B**) and (**C**) Immunohistochemical staining for the proliferation marker pH3 (arrows) and astrocytic differentiation marker S100B (arrowheads) in tumours from HGA-Control (A), HGA-Nfia$^{flox}$ (B) and HGA-Nfib$^{flox}$ (C). (**D**) Quantification of pH3-positive cells reveals no significant difference in proliferation between HGA models (Mann-Whitney U test). (**E**) Quantification of S100B-positive cells demonstrates a decrease of astrocytic differentiation in HGA-Nfia$^{flox}$ and HGA-Nfib$^{flox}$ tumours. Scale bar in (C) high power = 50 μm; low power = 200 μm. Error bars in (D) and (E) depict mean ± SEM.

and HGA-Nfib$^{flox}$ mice, this difference did not reach significance (Mann–Whitney *U* test; Figure 4D and Table S5, available at *Carcinogenesis* Online). In contrast, the number of S100B-positive cells was significantly reduced in both *Nfi* deletion models as compared to HGA-Control tumours ($P = 0.0076$ and $P = 0.0104$; Mann–Whitney *U* test; Figure 4E). This consequently leads to a reduction in the ratio of proliferating to differentiated cells (Table S5, available at *Carcinogenesis* Online). This reduction of differentiated tumour cells in comparison to proliferating cells suggest that *Nfi* deletion leads to a less differentiated phenotype.

We further assessed these tumour models by investigating other markers of tumour aggression. As an increased number of irregular, hyperchromatic nuclei is associated with more aggressive tumours, we quantified the number of these nuclei in Ki-67 stained sections counterstained with H&E (Figure 5A–C and Table S6, available at *Carcinogenesis* Online). As expected, the number of cells with hyperchromatic nuclei was increased over five times in HGA-Nfia$^{flox}$ and HGA-Nfib$^{flox}$ tumours as compared to the HGA-Control ($P = 0.0078$ and 0.0019; Mann–Whitney *U* test; Figure 5D and Table S6, available at *Carcinogenesis* Online). Another sign of tumour aggression is local invasion of tumour cells into the surrounding tissue. Therefore, we analysed the tumour borders within the whole series of rostral to caudal coronal sections stained for Ki-67 and counterstained with H&E to determine the number of tumours with invasion into normal brain tissue (Figure 5E–G). We performed this quantification for each tumour (Figure 5H), as well as for each mouse irrespective of the number of tumours it harboured (Figure 5I). In both analyses, more local invasion was significantly observed in HGA-Nfia$^{flox}$ and HGA-Nfib$^{flox}$ mice (Chi-square with Yates' correction; Table S7, available at *Carcinogenesis* Online). These results indicate that loss of either *Nfia* or *Nfib* results in more aggressive tumours.

## HGA-Nfia$^{flox}$ and HGA-Nfib$^{flox}$ mouse tumours model human glioblastoma

To compare our mouse model tumours to human disease, a neuropathologist blindly assessed serial sections stained for

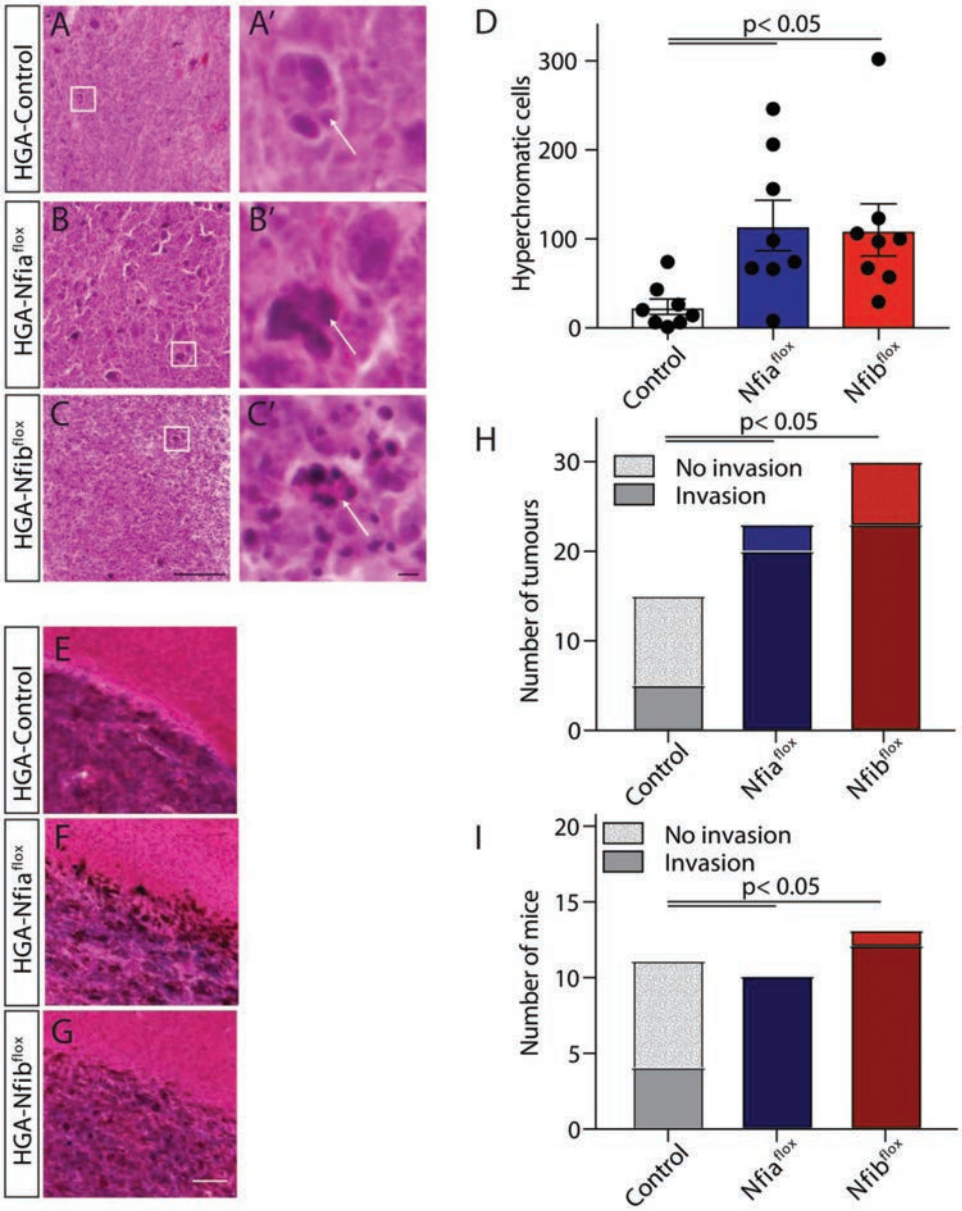


**Figure 5.** Tumours from HGA-Nfia$^{flox}$ or HGA-Nfib$^{flox}$ display more aggressive pathology. (**A**), (**B**) and (**C**) Representative images of hyperchromatic and multinucleated cells in Ki67-stained (brown cells) sections, counterstained with H&E of tumours from HGA-Control (A), HGA-Nfia$^{flox}$ (B) and HGA-Nfib$^{flox}$ mice (C). (**D**) Quantification reveals an increase of these neoplastic cells in tumours from HGA-Nfia$^{flox}$ and HGA-Nfib$^{flox}$ mice (**$P \leq 0.01$; Mann–Whitney *U* test). (**E**), (**F**) and (**G**) Representative images of the tumour border from the Ki67-stained (brown cells) sections, counterstained with H&E shown in Figure 3A for HGA-Control (E), HGA-Nfia$^{flox}$ (F) and HGA-Nfib$^{flox}$ mice (G). Note that the border is broken by invading cells in the tumours of the HGA-Nfi$^{flox}$ models. (**H**) Number of tumour masses per HGA model with diffuse borders and locally invading cells (invasion) reveals an increased number of tumours with diffuse borders when *Nfia* or *Nfib* is deleted (**$P \leq 0.01$ and *$P \leq 0.05$; Chi-square with Yates' correction). (**I**) This also holds true when assessed per mouse (**$P \leq 0.01$ and *$P \leq 0.05$; Chi-square with Yates' correction). Scale bar in (C) = 200 μm, in (C′) = 10 μm, in (G) = 1000 μm and in (G′) = 100 μm. Error bars in (D) depict mean ± SEM.

H&E. As originally reported, all tumours in the HGA-control models displayed pathological features of human glioblastoma, including the presence of mitotic cells and necrosis (27). In addition, the presence of haemorrhage, parenchymal and corpus callosum invasion, ependymal spread and pleomorphism (Table S8, available at *Carcinogenesis* Online) were also assessed. Tumours from both the HGA-Nfia$^{flox}$ and HGA-Nfib$^{flox}$ models encompassed the same histological variation as HGA-control, confirming that the absence of either *Nfi* family member does not alter histologic tumour grade.

When assessing the relationship between the neuropathological features and tumour models, no correlation was observed for the presence of necrosis or haemorrhage with the models (Spearman correlation test; Figure 6A, Table S9, available at *Carcinogenesis* Online). Invasion and spread were more associated with tumours from HGA-*Nfi* mice, in line with a more aggressive tumour pathology. A more pronounced difference was observed for cellular pleomorphism. While only 6 out of 10 tumours from HGA-Control mice displayed severe cellular pleomorphism, 10 out of 10 and 12 out of 13 in HGA-Nfia$^{flox}$ and HGA-Nfib$^{flox}$

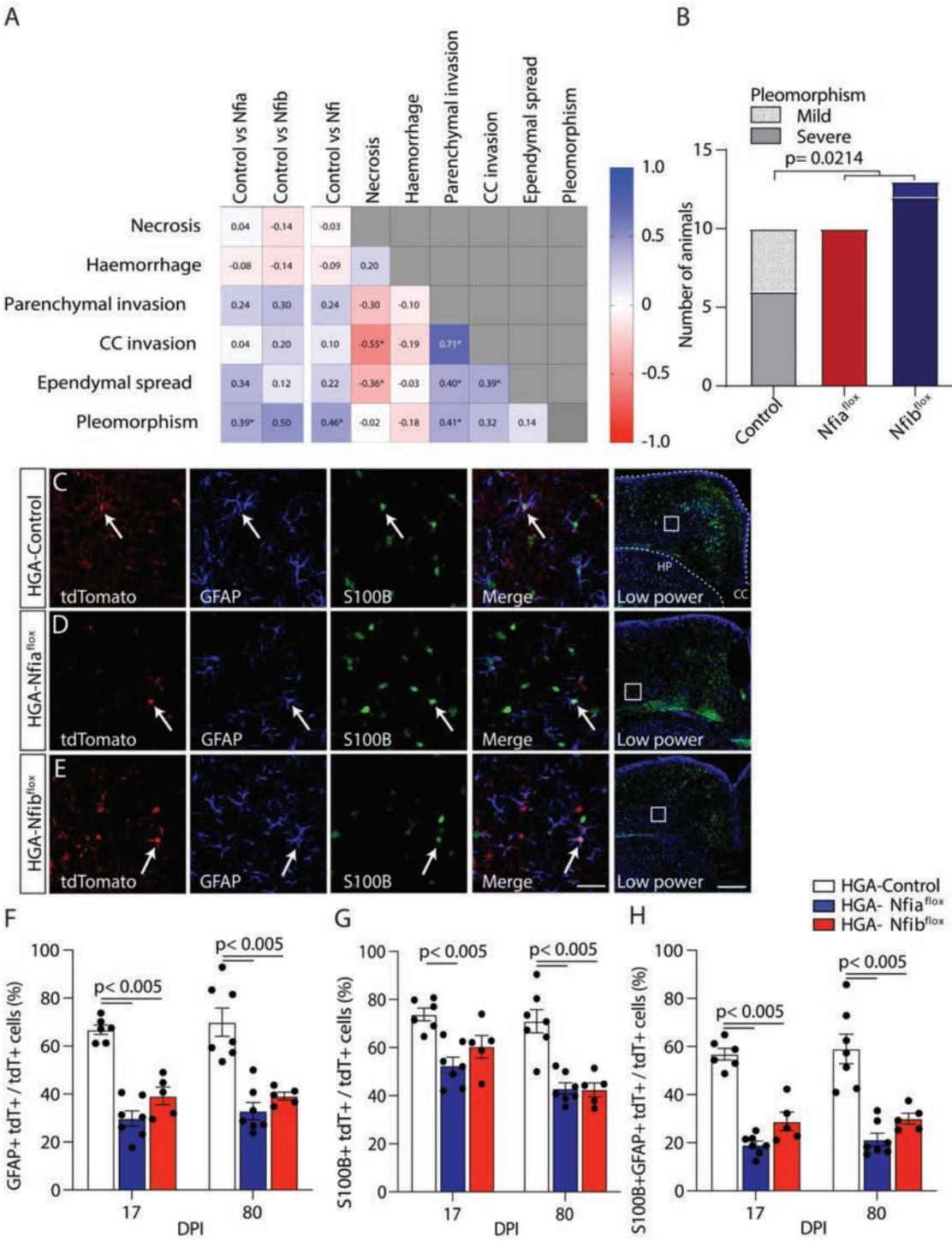


**Figure 6.** Neuropathological features of tumours arising in HGA mouse models. (**A**) Correlation matrix of neuropathological features. Ependymal spread, parenchymal invasion and corpus callosum (CC) invasion were positively correlated with each other. Cellular pleomorphism strongly correlated with *Nfi* deletion. Numbers and colours represent the Spearman correlation (*r*), while * indicates a significant correlation with $P < 0.05$. (**B**) Number of animals for each mouse model displaying mild or severe abundance of pleomorphism within the tumour. (**C**), (**D**) and (**E**) Immunohistochemical analyses at 80 days post injection (DPI) with tamoxifen. In all three HGA models, co-staining of tdTomato, GFAP and S100B is observed (Arrow). (**F**), (**G**) and (**H**) Quantification of GFAP-positive (F), S100B-positive (G) and double positive (H) cells reveal that less tdTomato-positive cells in the cortex of HGA-Nfia$^{flox}$ and HGA-Nfib$^{flox}$ mice co-express astrocytic markers at 17- and 80-days post injection. Scale bar in (E) high power = 100 μm; low power = 1000 μm. CC, corpus callosum; HP, hippocampus. Error bars in (F), (G) and (H) depict mean ± SEM.

tumours, respectively, featured severe pleomorphism ($P = 0.025$ and 0.067; Spearman correlation test; Figure 6B). Together, these results indicate that NFIA and NFIB function as tumour suppressors and loss is associated with more aggressive phenotypes.

## Nfi deletion results in early loss of glial differentiation markers

Based on the immunofluorescent analyses, loss of *Nfi* results in less differentiated tumours. This is in line with ectopic

expression of NFIA or NFIB leading to increased expression of astrocytic marker genes (10,12,14). As loss of either *Nfia* or *Nfib* in developmental models results in delayed and reduced astrogliogenesis, the question arises whether reduced expression of astrocytic markers in HGA-Nfia$^{flox}$ and HGA-Nfib$^{flox}$ is an early event or only occurs in the final phase of tumorigenesis (4,6,41–43).

To determine early changes in astrocytic differentiation, brains from the three HGA models were collected at 17- and 80-days post injection (DPI) of tamoxifen. Seventeen days post injection is 3 days after the final injection, while 80 days post injection is prior to any clinical sign having been observed in the HGA models. In the collected brains for both stages, the cortex did not harbour any tumour masses or proliferating tdTomato-positive cells. Matching coronal sections were stained for tdTomato, S100B, and GFAP to assess co-expression (Figure 6C–E). Compared to HGA-Control brains, less tdTomato-positive cells co-expressed S100B, GFAP or both astrocytic markers in HGA-Nfia$^{flox}$ and HGA-Nfib$^{flox}$ cortex at either time point (Figure 6F–H and Table S10, available at *Carcinogenesis* Online). Although the difference is more pronounced at DPI 80, no significant reduction was observed when compared 17- and 80-days post injection for each model, with the exception of a small reduction in tdTomato-positive cells co-expressing S100B in HGA-Nfib$^{flox}$ brain. Therefore, the loss of astrocytic markers seems to be a very early event after recombination which remains stable as tumorigenesis proceeds. This is in line with the results from a two-way ANOVA analyses, showing that the majority of the variation is explained by the HGA model rather than the collection point or the interaction between both. There are no differences between HGA-Nfia$^{flox}$ and HGA-Nfib$^{flox}$, further indicating that both NFI proteins function similarly within this context.

## Discussion

In the present study, we identified that the transcription factors NFIA and NFIB function as tumour suppressors in the pathophysiology of HGA. Tumour-specific deletion of either family member in our HGA mouse model resulted in more aggressive tumours compared to those observed in HGA-Control mice. Tumours developed earlier in HGA-Nfia$^{flox}$ and HGA-Nfib$^{flox}$ mice, while they also presented with larger and more tumour masses. These tumours were classified histologically as glioblastoma and displayed pathologic features suggestive of more aggressive behaviour: cellular pleomorphism and invasion of surrounding tissue, fewer differentiated cells, more hyperchromatic nuclei and more diffuse tumour borders.

Building on previous insertional mutagenesis mouse models and expression data, our results now provide conclusive evidence for an independent tumour suppressive role for NFI transcription factors in high-grade glioma (10,14,16,25,26). Even though in our HGA mouse model the receptor kinase, P53 and RB signalling pathways are already disrupted by deletion of *Pten*, *Tp53* and *Rb1*, respectively, additional loss of either *Nfi* gene still contributed significantly to the pathophysiology of these tumours. This implies that the NFI proteins function, at least partly, independent of these three pathways that are commonly affected in glioma. Further investigation will be required to delineate the precise genes and pathways regulated by NFIA and NFIB that are responsible. However, as there are no clear differences between tumours arising from HGA-Nfia$^{flox}$ and HGA-Nfib$^{flox}$, these downstream pathways may be very similar, mimicking the overlap in the function of NFIA and NFIB in glial development (3). While redundant in function, we previously found that double-knockout of Nfis resulted in a more severe brain developmental phenotype, and therefore we suspect that an overall allelic dosage may also be important to consider in the context of NFIs in cancer when further delineating their molecular mechanisms (3).

An intrinsic tumour suppressive role likely extends to other brain tumours arising for tissues in which the NFI proteins regulate development. In three independent insertional mutagenesis models for SHH-subtype medulloblastomas, at least 51 out of 139 (47%), 29 out of 41 (59%) and 40 out of 85 (47%) tumours harboured insertions in a *Nfi* locus (44–46). For NFIA, an independent role has been implicated; heterozygous deletion of *Nfia* in mice with heterozygous cerebellum-specific deletion of *Ptch1* have an increased tumour incidence from 37.5% to 61.9% and a reduced tumour latency from 189 to 128 days post induction in these mice (45). An increased tumour incidence might underlie the presence of multiple tumour masses in the HGA-Nfia$^{flox}$ and HGA-Nfib$^{flox}$ model. For ependymoma of the ST-EPN-YAP1 molecular subtype, the role of NFI proteins is less straight forward. In this subtype, interaction between the YAP1-MAMLD1 fusion protein and NFIA and NFIB seems to be required for its role as an oncogenic driver (47). Thus, while the normal NFI regulated pathway may favour differentiation, YAP1-MAMLD1 protein changes this transcriptional complex and therefore transcriptional regulation. Whether NFI also acts as a tumour suppressor in other tumour types requires further investigation.

In contrast to the medulloblastoma mouse model, in which all cells are heterozygous for *Nfia*, deletion of *Nfia* or *Nfib* only occurs after induction in GFAP-positive cells in our HGA models. This inducible deletion model provided exquisite control over the induction of endogenous tumours in a cell autonomous manner, uncoupling their specific tumour suppressor role from the role of NFI proteins during brain development. Our results also demonstrate that similar to the mouse medulloblastoma model described above, the tumour suppressive role of NFI proteins is context-dependent, and in our experiments required the HGA model background to be revealed. Loss of a single *Nfi* family member in isolation is not sufficient to induce tumour formation (data not shown). Currently, no tumours have been reported in human individuals with germline *NFI* haploinsufficiency, although the cohort might be too limited to assess any increased tumour risk (48). Similarly, no brain tumours have been reported for any of the heterozygous knockout or homozygous conditional knockout models.

The precise underlying mechanism by which loss of *NFIA* or *NFIB* contributes to more aggressive tumours requires further investigation, but could be related to its function in glial differentiation. This may contribute to tumorigenesis and progression at different stages. Loss of astrocytic markers occurs very early in the HGA-Nfia$^{flox}$ and HGA-Nfib$^{flox}$ models and could alter astrocytic morphology, in line with that observed after astrocyte specific deletion of *Nfia* (49). This may be a crucial step in the transformation of healthy cells into tumorigenic cells and therefore lead to multiple tumour masses in these models due to an increased rate of transformation. In growing tumours, reduced potential to differentiate can result in faster growth and increased cell migration (50).

In conclusion, we demonstrated that both NFIA and NFIB function as tumour suppressors in high-grade glioma. The high-grade glioma model we used requires the deletion of three tumour suppressor genes, *Pten*, *Rb1* and *Tp53*, none of which function on their own to cause tumorigenesis in mice. Similarly, loss of NFI on its own is not sufficient to initiate transformation. However, in combination with loss of these tumour suppressors,

loss of *Nfi* function significantly worsens pathological outcomes. Future investigations into the downstream molecular mechanisms involved will help delineate the role of NFI proteins in high-grade glioma and other tumour types, and pave the way for improved diagnostic and therapeutic approaches to high-grade glioma.

## Supplementary material

Supplementary data are available at *Carcinogenesis* online.

## Funding

The research was funded by the National Health and Medical Research Council (Grant numbers GNT1100443, GNT1120615 to L.J.R.); Tour de Cure (Scott Canner Young Research Grant to J.B.); the Brain Foundation (Research gift to J.B.); Ride for Rhonda (Research gift to L.J.R. and J.B.); and NYSTEM (Contract C030133 to R.M.G.). Students were supported by the University of Queensland (International Postgraduate Student Scholarship to K.S.C., UQ Queensland Graduate School Scholarship to Z.L., UQ Centennial Scholarship to J.W.C.L.); Australian Government (Research Training Program Scholarship to J.W.C.L.); and the Royal College of Pathologists of Australasia (Medical Student Scholarship to Z.L.).

## Acknowledgements

We thank Dr Caitlin R. Bridges for contributing to data acquisition and histology and the staff of the University of Queensland Biological Resources (UQBR) animal facility and QBI Advanced Microscopy and Analysis Facility for their expertise and assistance in this project. We thank Alan Ho for statistical assistance. We thank Professor Suzanne J. Baker, St Jude Children's Research Hospital, USA, for providing the high-grade glioma mouse line used in these studies.
*Conflict of Interest Statement*: None declared.

## Data availability

The data underlying this article are available in the article and in its online Supplementary Material.

## References

1. Marosi, C. *et al.* (2017) Milestones of the last 10 years: CNS cancer. *Memo*, 10, 18–21.
2. Laug, D. *et al.* (2018) A glial blueprint for gliomagenesis. *Nat. Rev. Neurosci.*, 19, 393–403.
3. Bunt, J. *et al.* (2017) Combined allelic dosage of Nfia and Nfib regulates cortical development. *Brain Neurosci. Adv.*, 1, 2398212817739433.
4. Piper, M. *et al.* (2010) NFIA controls telencephalic progenitor cell differentiation through repression of the Notch effector Hes1. *J. Neurosci.*, 30, 9127–9139.
5. Shu, T. *et al.* (2003) Abnormal development of forebrain midline glia and commissural projections in Nfia knock-out mice. *J. Neurosci.*, 23, 203–212.
6. Gobius, I. *et al.* (2016) Astroglial-mediated remodeling of the interhemispheric midline is required for the formation of the corpus callosum. *Cell Rep.*, 17, 735–747.
7. Piper, M. *et al.* (2009) Multiple non-cell-autonomous defects underlie neocortical callosal dysgenesis in Nfib-deficient mice. *Neural Dev.*, 4, 43.
8. Caiazzo, M. *et al.* (2015) Direct conversion of fibroblasts into functional astrocytes by defined transcription factors. *Stem Cell Reports*, 4, 25–36.
9. Tchieu, J. *et al.* (2019) NFIA is a gliogenic switch enabling rapid derivation of functional human astrocytes from pluripotent stem cells. *Nat. Biotechnol.*, 37, 267–275.
10. Stringer, B.W. *et al.* (2016) Nuclear factor one B (NFIB) encodes a subtype-specific tumour suppressor in glioblastoma. *Oncotarget*, 7, 29306–29320.
11. Bisgrove, D.A. *et al.* (2000) Regulation of brain fatty acid-binding protein expression by differential phosphorylation of nuclear factor I in malignant glioma cell lines. *J. Biol. Chem.*, 275, 30668–30676.
12. Brun, M. *et al.* (2009) Nuclear factor I regulates brain fatty acid-binding protein and glial fibrillary acidic protein gene expression in malignant glioma cell lines. *J. Mol. Biol.*, 391, 282–300.
13. Brun, M. *et al.* (2018) Nuclear factor I represses the notch effector HEY1 in glioblastoma. *Neoplasia*, 20, 1023–1037.
14. Chen, K.S. *et al.* (2020) Transcription factors NFIA and NFIB induce cellular differentiation in high-grade astrocytoma. *J. Neurooncol.*, 146, 41–53.
15. Glasgow, S.M. *et al.* (2014) Mutual antagonism between Sox10 and NFIA regulates diversification of glial lineages and glioma subtypes. *Nat. Neurosci.*, 17, 1322–1329.
16. Song, H.R. *et al.* (2010) Nuclear factor IA is expressed in astrocytomas and is associated with improved survival. *Neuro. Oncol.*, 12, 122–132.
17. Brawley, V.S. *et al.* (2013) The miR-223/nuclear factor I-A axis regulates glial precursor proliferation and tumorigenesis in the CNS. *J. Neurosci.*, 33, 13560–13568.
18. Lee, J.S. *et al.* (2014) A novel tumor-promoting role for nuclear factor IA in glioblastomas is mediated through negative regulation of p53, p21, and PAI1. *Neuro Oncol.*, 16, 191–203.
19. Kang, P. *et al.* (2012) Sox9 and NFIA coordinate a transcriptional regulatory cascade during the initiation of gliogenesis. *Neuron*, 74, 79–94.
20. Chen, K.S. *et al.* (2017) The convergent roles of the nuclear factor I transcription factors in development and cancer. *Cancer Lett.*, 410, 124–138.
21. Brat, D.J. *et al.*; Radiation Therapy Oncology Group. (2004) Analysis of 1p, 19q, 9p, and 10q as prognostic markers for high-grade astrocytomas using fluorescence in situ hybridization on tissue microarrays from Radiation Therapy Oncology Group trials. *Neuro Oncol.*, 6, 96–103.
22. Brennan, C.W. *et al.*; TCGA Research Network. (2013) The somatic genomic landscape of glioblastoma. *Cell*, 155, 462–477.
23. [dataset] The Cancer Genome Atlas Research Network. (2008) Comprehensive genomic characterization defines human glioblastoma genes and core pathways. *Nature*, 455, 1061–1068.
24. Brat, D.J. *et al.* (2015) Comprehensive, integrative genomic analysis of diffuse lower-grade gliomas. *N. Engl. J. Med.*, 372, 2481–2498.
25. Johansson, F.K. *et al.* (2004) Identification of candidate cancer-causing genes in mouse brain tumors by retroviral tagging. *Proc. Natl. Acad. Sci. U. S. A.*, 101, 11334–11337.
26. Vyazunova, I. *et al.* (2014) Sleeping Beauty mouse models identify candidate genes involved in gliomagenesis. *PLoS One*, 9, e113489.
27. [dataset] Chow, L.M.L. *et al.* (2011) Cooperativity within and among Pten, p53, and Rb pathways induces high-grade astrocytoma in adult brain. *Cancer Cell*, 19, 305–316.
28. Suzuki, A. *et al.* (2001) T cell-specific loss of Pten leads to defects in central and peripheral tolerance. *Immunity*, 14, 523–534.
29. Marino, S. *et al.* (2000) Induction of medulloblastomas in p53-null mutant mice by somatic inactivation of Rb in the external granular layer cells of the cerebellum. *Genes Dev.*, 14, 994–1004.
30. Madisen, L. *et al.* (2010) A robust and high-throughput Cre reporting and characterization system for the whole mouse brain. *Nat. Neurosci.*, 13, 133–140.
31. Clark, B.S. *et al.* (2019) Single-Cell RNA-Seq analysis of retinal development identifies NFI factors as regulating mitotic exit and late-born cell specification. *Neuron*, 102, 1111–1126.e5.
32. Chang, C.Y. *et al.* (2013) NFIB is a governor of epithelial-melanocyte stem cell behaviour in a shared niche. *Nature*, 495, 98–102.
33. Schanze, I. *et al.* (2018) NFIB haploinsufficiency is associated with intellectual disability and macrocephaly. *Am. J. Hum. Genet.*, 103, 752–768.
34. Schindelin, J. *et al.* (2012) Fiji: an open-source platform for biological-image analysis. *Nat. Methods*, 9, 676–682.
35. Chen, K.S. *et al.* (2017) Differential neuronal and glial expression of nuclear factor I proteins in the cerebral cortex of adult mice. *J. Comp. Neurol.*, 525, 2465–2483.
36. Bunt, J. *et al.* (2010) Regulation of cell cycle genes and induction of senescence by overexpression of OTX2 in medulloblastoma cell lines. *Mol. Cancer Res.*, 8, 1344–1357.

37. [dataset] Gusev, Y. *et al*. (2018) The REMBRANDT study, a large collection of genomic data from brain cancer patients. *Sci. Data*, 5, 180158.
38. [dataset] Gravendeel, L.A.M. *et al*. (2009) Intrinsic gene expression profiles of gliomas are a better predictor of survival than histology. *Cancer Res.*, 69, 9065–9072.
39. Huang, D.W. *et al*. (2009) Systematic and integrative analysis of large gene lists using DAVID bioinformatics resources. *Nat. Protoc.*, 4, 44–57.
40. Houston, Z.H. *et al*. (2020) Understanding the uptake of nanomedicines at different stages of brain cancer using a modular nanocarrier platform and precision bispecific antibodies. *ACS Cent. Sci.*, 6, 727–738.
41. Barry, G. *et al*. (2008) Specific glial populations regulate hippocampal morphogenesis. *J. Neurosci.*, 28, 12328–12340.
42. Matuzelski, E. *et al*. (2017) Transcriptional regulation of Nfix by NFIB drives astrocytic maturation within the developing spinal cord. *Dev. Biol.*, 432, 286–297.
43. Namihira, M. *et al*. (2009) Committed neuronal precursors confer astrocytic potential on residual neural precursor cells. *Dev. Cell*, 16, 245–255.
44. Wu, X. *et al*. (2012) Clonal selection drives genetic divergence of metastatic medulloblastoma. *Nature*, 482, 529–533.
45. Genovesi, L.A. *et al*. (2013) Sleeping Beauty mutagenesis in a mouse medulloblastoma model defines networks that discriminate between human molecular subgroups. *Proc. Natl. Acad. Sci. U. S. A.*, 110, E4325–E4334.
46. Lastowska, M. *et al*. (2013) Identification of a neuronal transcription factor network involved in medulloblastoma development. *Acta Neuropathol. Commun.*, 1, 35.
47. Pajtler, K.W. *et al*. (2019) YAP1 subgroup supratentorial ependymoma requires TEAD and nuclear factor I-mediated transcriptional programmes for tumorigenesis. *Nat. Commun.*, 10, 3914.
48. Zenker, M. *et al*. (2019) Variants in nuclear factor I genes influence growth and development. *Am. J. Med. Genet. C. Semin. Med. Genet.*, 181, 611–626.
49. Huang, A.Y.-S. *et al*. (2020) Region-specific transcriptional control of astrocyte function oversees local circuit activities. *Neuron*, 106, 992–1008.e9.
50. Vo, T.M. *et al*. (2019) A positive feedback loop involving nuclear factor IB and calpain 1 suppresses glioblastoma cell migration. *J. Biol. Chem.*, 294, 12638–12654.